

LETTER TO THE EDITOR

A stringent upper limit of the PH₃ abundance at the cloud top of Venus

T. Encrenaz¹, T. K. Greathouse², E. Marcq³, T. Widemann¹, B. Bézard¹, T. Fouchet¹, R. Giles², H. Sagawa⁴, J. Greaves⁵, and C. Sousa-Silva⁶

¹ LESIA, Observatoire de Paris, PSL Université, CNRS, Sorbonne Université, Université de Paris, 92195 Meudon, France

² SwRI, Div. 15, San Antonio, TX 78228, USA

³ LATMOS/IPSL, UVSQ Université Paris-Saclay, Sorbonne Université, CNRS, 78280 Guyancourt, France

⁴ Kyoto Sanyo University, Kyoto 603-855, Japan

⁵ School of Physics and Astronomy, Cardiff University, Cardiff, UK

⁶ Department of Earth, Atmospheric and Planetary Sciences, Massachusetts Institute of Technology, Cambridge, MA, USA

Received September 30, 2020, revised October 14, 2020

ABSTRACT

Aims. Following the announcement of the detection of phosphine (PH₃) in the cloud deck of Venus at millimeter wavelengths, we have searched for other possible signatures of this molecule in the infrared range.

Methods. Since 2012, we have been observing Venus in the thermal infrared at various wavelengths to monitor the behavior of SO₂ and H₂O at the cloud top. We have identified a spectral interval recorded in March 2015 around 950 cm⁻¹ where a PH₃ transition is present.

Results. From the absence of any feature at this frequency, we derive, on the disk-integrated spectrum, a 3- σ upper limit of 5 ppbv for the PH₃ mixing ratio, assumed to be constant throughout the atmosphere. This limit is 4 times lower than the disk-integrated mixing ratio derived at millimeter wavelengths.

Conclusions. Our result brings a strong constraint on the maximum PH₃ abundance at the cloud top and in the lower mesosphere of Venus.

Key words. Planets and satellites: atmospheres – techniques: imaging spectroscopy – Infrared: planetary systems

1. Introduction

The atmospheric chemistry of Venus is driven by the cycles of water and sulfur dioxide (Krasnopolsky 1986, 2007, 2010; Mills et al. 2007; Zhang et al. 2012). Below the clouds, both species are present with relatively large abundances (about 30 ppmv and 130 ppmv respectively, Bézard and De Bergh 2007, Marcq et al. 2013) and, at low latitude, are transported upward by Hadley convection. Their abundances drop drastically above the H₂SO₄ clouds, formed after the SO₂ photodissociation and the combination of SO₃ with H₂O. Their abundances in the mesosphere are about 1–3 ppmv (Fedorova et al. 2008; Belyaev et al. 2012) and 10–1000 ppbv (Zasova et al. 1993; Marcq et al. 2013, 2020; Vandaele et al. 2017a, b; Encrenaz et al. 2020) respectively. The water and sulfur dioxide cycles have been extensively monitored over several decades, using Pioneer Venus, the Venera 15 spacecraft, Venus Express and Akatsuki by imaging and spectroscopy in the ultraviolet and infrared ranges. Since 2012, we have been monitoring the abundances of SO₂ and H₂O (by observing HDO as a proxy) using ground-based imaging spectroscopy in the thermal infrared range with the TEXES (Texas Echelon Cross Echelle Spectrograph) imaging spectrometer, mounted at the Infrared Telescope Facility at Maunakea Observatory (Encrenaz et al. 2020).

In September 2020, the detection of phosphine (PH₃) in the cloud decks of Venus was reported on the basis of millimeter

heterodyne spectroscopy measurements using both the JCMT and the ALMA facilities (Greaves et al. 2020). This result was a big surprise, as the presence of phosphine is not expected in an oxidized atmosphere, like the ones of the terrestrial planets, if abiotic processes only are considered.

Since the detection of PH₃ was based on the identification of a single transition (at a wavelength of 1.123 mm), we searched for other possible spectral signatures at other wavelengths to confirm and complement the first detection. Phosphine has a very rich infrared spectrum, which ranges from the near-infrared range up to the thermal range. As shown in our previous monitoring of SO₂ and H₂O, the simultaneous observation of the minor species and weak CO₂ lines is needed to infer the mixing ratio of the species. A good compromise can be found in the 930–960 cm⁻¹ region, which includes PH₃ transitions with an intensity close to 10⁻²⁰ cm⁻¹/molec.cm⁻² and CO₂ lines of various intensities. Within our data set, we found a spectral region around 955 cm⁻¹ which includes some relatively strong transitions of PH₃ and weak transitions of CO₂. We recorded the 951–956 cm⁻¹ spectrum with the purpose of analyzing the CO₂ hot band for temperature retrieval and for an analysis of the non-LTE effects. Three data sets were obtained in February 2014, March 2015 and January 2016. One PH₃ transition is usable in the March 2015 data set and we analyzed it to derive an upper limit of the PH₃ mixing ratio; in the two other cases, the PH₃ transition fell in the overlap between two consecutive orders of the TEXES instrument (Lacy et al. 2002).

Send offprint requests to: T. Encrenaz

In this paper, we first describe the observations (Section 2). An upper limit of the PH_3 abundance at the cloud top is presented in Section 3. Results are discussed in Section 4.

2. Observations

TEXES (Texas Echelon Cross Echelle Spectrograph) is an imaging high-resolution thermal infrared spectrograph in operation at the NASA InfraRed telescope Facility at Maunakea Observatory, Hawaii (Lacy et al. 2002), which combines high spectral capabilities ($R = 80000$ at $7\ \mu\text{m}$) and spatial capabilities (around $1\ \text{arcsec}$).

Data were recorded on March 28, 2015, at 01:21:14 UT, between 951 and $956\ \text{cm}^{-1}$. The Venus diameter was $14\ \text{arcsec}$ and the airmass was 1.016 . The Doppler velocity was $-11\ \text{km/s}$, corresponding to a Doppler shift of $+0.035\ \text{cm}^{-1}$ at $950\ \text{cm}^{-1}$. The illuminated fraction was 78% (very similar to the JCMT and ALMA observations reported by Greaves et al. (2020), and the evening terminator was observed. The slit length was $8\ \text{arcsec}$ and the slit width was $1.1\ \text{arcsec}$ at $950\ \text{cm}^{-1}$. We aligned the slit along the North-South celestial axis and we shifted it from west to east, with a step of half the slit width and an integration time of 2 seconds per position, to cover the planet in longitude from limb to limb, and to add a few pixels on the sky beyond each limb for sky subtraction. As the diameter of Venus was larger than the slit length, we made two scans (North and South) to cover the full latitude range with some overlap around the equator. The total observation time was 18 minutes. The atmospheric transmission is very good around $950\ \text{cm}^{-1}$; a single broad feature is observed at $955.25\ \text{cm}^{-1}$ (rest frequency) due to terrestrial atmospheric water vapor, which is outside the position of the PH_3 transition.

The TEXES data cubes were calibrated using the standard radiometric method (Lacy et al. 2002, Rohlf and Wilson 2004). Calibration frames consisting of black chopper blade measurements and sky observations are systematically taken before each observing scan, and the difference (black-sky) is taken as a flat field. If the temperature of the black blade, the telescope and the sky are equal, this method corrects both telescope and atmospheric emissions.

Figure 1 shows two disk-integrated spectra of Venus, with and without the limb contribution, along with a synthetic spectrum corresponding to a PH_3 volume mixing ratio of 20 ppbv, constant with altitude (details on the modeling are given in the following section). The strongest PH_3 transitions are located between 954 and $956.5\ \text{cm}^{-1}$ (Table 1). The doublet at $956.23\ \text{cm}^{-1}$ falls within a strong CO_2 line, so the useful spectral range is limited to 954 - $956\ \text{cm}^{-1}$. The two strongest PH_3 transitions fall in the wings of a strong CO_2 line; in addition, the one at $954.445\ \text{cm}^{-1}$ coincides with a discontinuity due to an overlap between two consecutive orders. The only usable PH_3 transition occurs at $955.23\ \text{cm}^{-1}$, and is free of instrumental contamination.

Both TEXES spectra show an emission core at the center of the strong CO_2 line at $954.545\ \text{cm}^{-1}$. This phenomenon is due to a non-LTE effect in the hot band of CO_2 around $955\ \text{cm}^{-1}$ (Table 1), which takes place in the upper mesosphere. Individual spectra show that the core emission is especially strong at the limb, but is still slightly present at the center of the disk. In order to minimize at maximum its effect on our analysis (which probes the few kilometers above the cloud top), we have integrated the TEXES data taking into account only the air-masses lower than 1.7, to exclude the limb and the high latitudes contributions. Our summation includes all latitude ranges up to $\pm 50^\circ$. This spectrum is used for the present analysis. It can be noticed that both

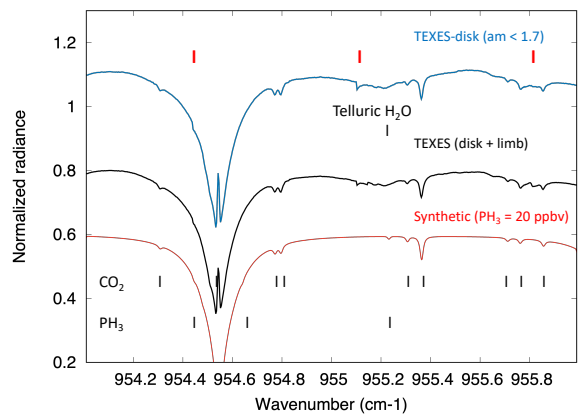


Fig. 1. Blue curve: the TEXES spectrum recorded on March 28, 2015 between 954 and $956\ \text{cm}^{-1}$, integrated for all air-masses lower than 1.7. Black curve (shifted by -0.2 for clarity): the TEXES disk-integrated spectrum of Venus, extracted from the same data set, including the limb contribution. Red curve (shifted by -0.4 for clarity): synthetic spectrum including CO_2 and PH_3 with a volume mixing ratio of 20 ppbv, constant with altitude, calculated for an airmass of 1.15 (30° latitude). The broad absorption feature around $955.215\ \text{cm}^{-1}$ is due to a telluric water vapor line. The red ticks at the top of the figure indicate the discontinuities due to an overlap between two consecutive orders.

TEXES spectra show no significant difference in the vicinity of the PH_3 line, with, in both cases, a signal-to-noise close to 1000 (see below).

3. PH_3 upper limit

Synthetic spectra of PH_3 in the atmosphere of Venus were calculated using the radiative transfer code that we apply for monitoring SO_2 and HDO at the cloud top (Encrenaz et al. 2016, 2019). This line-by-line code calculates the outgoing flux using an integration over 175 atmospheric levels separated by $1\ \text{km}$. The cloud top is defined by a blackbody at a temperature of $235\ \text{K}$ and a pressure of $150\ \text{mbar}$. The thermal profile is the same as used in Encrenaz et al. (2016). The temperature is $210\ \text{K}$ at $11\ \text{km}$ above the cloud top ($P = 10\ \text{mbar}$), $187\ \text{K}$ at $21\ \text{km}$ above this level ($P = 1\ \text{mbar}$) and $180\ \text{K}$ for altitudes higher than $28\ \text{km}$ above this level (P lower than $0.2\ \text{mbar}$). The penetration level in the mid-infrared is governed by the extinction cross-section of the H_2SO_4 particles which constitute the upper cloud deck. As illustrated by Zasova et al. (1993), the values of this coefficient are very similar at $950\ \text{cm}^{-1}$ and at $1350\ \text{cm}^{-1}$, where our analysis of SO_2 and HDO was performed. The atmospheric model used in our previous analyses is thus suited for the present study.

The spectroscopic data for PH_3 were extracted from the GEISA-2015 database (Jacquinot-Husson et al. 2016). For the broadening coefficients PH_3 - CO_2 , in the lack of more precise information, we assumed, as we did for SO_2 and HDO (Encrenaz et al. 2016), an increase by a factor of 1.4 with respect to the air-broadening coefficients (Nakazawa and Tanaka 1982). As a verification, we estimated independently the broadening coefficient of our PH_3 line at $955.231\ \text{cm}^{-1}$ by using NH_3 as an analog, as done by Greaves et al. (2020) for the PH_3 millimeter line. The air-broadened HWHM (half-width at half-maximum) of our PH_3 transition at $954.232\ \text{cm}^{-1}$ is $0.0744\ \text{cm}^{-1}\ \text{atm}^{-1}$. The NH_3 transition with the same quantum numbers as our PH_3 transition (ν_2 , $J = 4$, $K = 3$) has an air-broadened HWHM of $0.1017\ \text{cm}^{-1}$. The $\text{HWHM}(\text{PH}_3)/\text{HWHM}(\text{NH}_3)$ is $0.0744/0.1017 = 0.732$. Using the polynomial described by Wilzewski et al. (2016), we infer

Molecule.	Wavenumber cm ⁻¹	Band identification	Line identification	Intensity cm molec ⁻¹	Energy cm ⁻¹	Broad. coef. cm ⁻¹ atm ⁻¹
PH ₃	954.44508	0100 0000	3 0 0A+ 4 0 0A+	1.343×10^{-20}	88.9959	0.1014
PH ₃	954.64090	0100 0000	3 1 0E 4 1 0E	1.262×10^{-20}	88.4658	0.1026
PH ₃	955.23186	0100 0000	3 2 0E 4 2 0E	1.02×10^{-20}	86.8739	0.1076
PH ₃	956.2288	0100 0000	3 3 0A- 4 3 0A-	6.09×10^{-21}	84.2149	0.1078
PH ₃	956.2288	0100 0000	3 3 0A- 4 3 0A+	6.09×10^{-21}	84.2149	0.1078
CO ₂	955.306951	000 11 100 01	P11E	6.663×10^{-27}	1426.0242	0.1076

Table 1. Spectroscopic parameters of the strongest PH₃ transitions between 949 and 959 cm⁻¹, extracted from the GEISA-2015 database. The CO₂ transition used in the calculations is also added. The line intensities correspond to a temperature of 296 K. The broadening coefficients (HWHM) refer to the broadening by CO₂.

a CO₂-broadened HWHM of 0.1537 cm⁻¹ atm⁻¹ for the NH₃ transition. We thus derive, for the CO₂ HWHM of our PH₃ transition, a value of $0.157 \times 0.732 = 0.112$ cm⁻¹ atm⁻¹, very close to the value listed in Table 1.

Figure 2 shows an enlargement of the disk-integrated TEXES spectrum of March 28, 2015 (without the limb contribution), in the vicinity of the PH₃ transition at 955.23 cm⁻¹, compared with synthetic spectra of CO₂ and PH₃, for volume mixing ratios of 5, 10 and 20 ppbv, constant with altitude. As mentioned above, the slope of the observed spectrum, around the position of the PH₃ line, is due to the presence of a broad H₂O telluric line. It can be seen that there is no trace of PH₃ absorption in the TEXES spectrum.

In order to derive an upper limit for the PH₃ abundance at the cloud top of Venus, we have assumed, as in the case of SO₂ and HDO, that the PH₃/CO₂ line depth ratio varies linearly with the PH₃ volume mixing ratio. In the case of Mars, we have shown that this method is valid for line depths weaker than ten percent for deriving H₂O₂ and HDO volume mixing ratios from H₂O₂/CO₂ and HDO/CO₂ line depth ratios; the uncertainty is a few percent for air-masses lower than 2 (Encrenaz et al. 2008, 2015a). In the case of Venus, we have shown that, in the 1350 cm⁻¹ range, for SO₂ and HDO lines weaker than ten percent in depth, the linearity is verified with an uncertainty of 7 percent for an air-mass of 1.4 (Encrenaz et al. 2012).

We estimated the peak-to-peak (3- σ) variations of the TEXES continuum in the vicinity of the PH₃ transition, between 955.20 and 955.27 cm⁻¹. We found a value of 0.001, corresponding to a S/N of about 1000. We checked that this high signal-to-noise ratio is actually achieved between the lines over the whole range of the spectrum (Figure 1). The CO₂ line depth in the TEXES spectrum is 0.01. The PH₃/CO₂ line depth ratio in the TEXES spectrum is thus lower than 0.10, while this ratio, in the synthetic spectrum, is 0.11 for a PH₃ volume mixing ratio of 5 ppbv. We thus infer a 3- σ upper limit of 5 ppbv for the PH₃ mixing ratio at the cloud top of Venus.

As a next step, we searched for possible local variations of the signal at the position of the PH₃ line over the disk of Venus. To do so, we used the same method as in the case of our SO₂ and HDO maps, which are derived from the SO₂/CO₂ and HDO/CO₂ line depth ratios, respectively. We defined the depth of the pseudo-PH₃ line by taking the signal at the line center, divided by the mean value of the continuum on each side of this position. We measured, in the same way, the depth of the CO₂ line at 955.3069 cm⁻¹, and we took the ratio of both quantities. The result is shown in Figure 3. It can be seen that the PH₃/CO₂ line depth ratio is always between +0.05 and -0.05, except at high southern latitudes where the ratio is close to 0.10. These high values are meaningless, because, at these latitudes, the CO₂ line depth is zero or negative, indicating a different behavior of

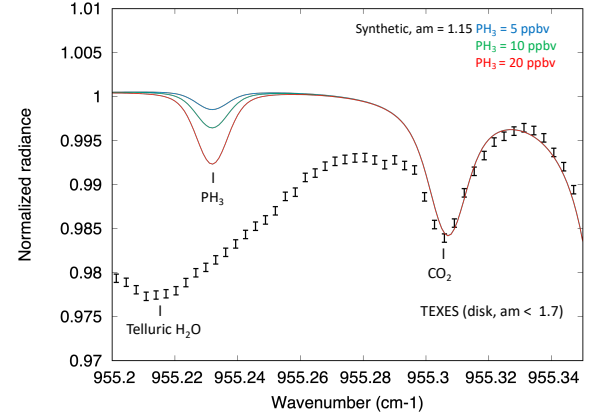


Fig. 2. Black error bars (3- σ): The disk-integrated spectrum of Venus (without the limb contribution) between 955.20 and 955.35 cm⁻¹ recorded on March 28, 2015. Models: CO₂ and PH₃ (blue: 5 ppbv; green: 10 ppbv; red: 20 ppbv), calculated for an airmass of 1.15 and for a constant PH₃ volume mixing ratio throughout the mesosphere. The slope of the TEXES spectrum is due to the broad telluric H₂O line centered at 955.215 cm⁻¹.

the temperature profile at the level of the southern polar collar. The upper limit for the PH₃ mixing ratio inferred from Figure 4 is 3.5 ppbv. The fact that this value is lower than our disk-integrated limit is due to the fact that, in the mapping process, the fluxes are averaged over 3 pixels, both at the line center and on each side of the line. This result confirms our 3- σ upper limit of 5 ppbv.

4. Discussion

Our upper limit of PH₃ is to be compared with the detection of phosphine in the millimeter range. Our upper limit is not compatible with a constant mixing ratio of 20 ppb throughout the mesosphere, as announced by Greaves et al. (2020). We might wonder if the difference between the two results could be due to the altitude difference of the regions probed at both wavelengths. Indeed, the continuum thermal emission at millimeter wavelengths probes an altitude around 55 km, i.e. within the clouds. This level is close to the one probed at 19 μ m, in the ν_2 band of SO₂ (in our model, $z = 57$ km, $P = 250$ mb, $T = 241$ K). The TEXES measurements at 10- μ m, like the 7- μ m observations of the ν_3 SO₂ band, probe the cloud top (in our present model, located at a pressure of 150 mbar and a temperature of 235 K, corresponding to an altitude of about 60 km; Encrenaz et al. 2016, 2019).

So we might wonder if a PH₃ vertical profile enriched in the upper cloud at 55 km and depleted above 60 km would resolve

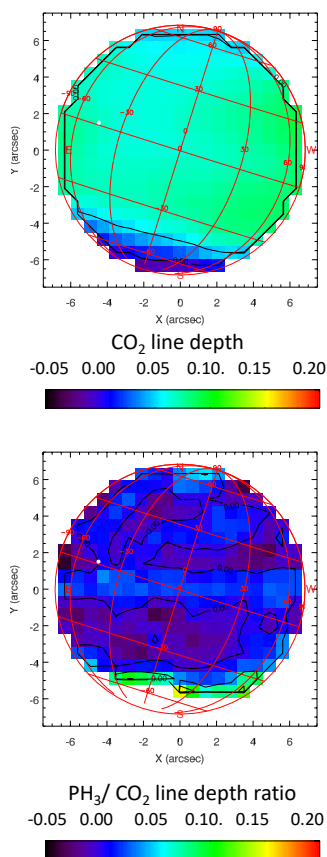


Fig. 3. Top: map of the line depth of the weak CO₂ transition at 955.3069 cm⁻¹, corresponding to the observations of March 28, 2015 shown in Figures 2 and 3. Bottom: map of the PH₃/CO₂ line depth ratio. The sub-solar point is shown as a white dot. The negative values in the map of the CO₂ line depth (top) indicate a different behavior of the temperature profile at the level of the polar collar, at high southern latitudes.

the discrepancy. However it is not the case, because the core of millimeter line is very narrow (less than about 20 MHz). If the PH₃ millimeter line was formed within the clouds, at a pressure level of 100 mbars or more, its HWHM would be at least 0.01 cm⁻¹, i.e. 300 MHz. Such a broad line would not be observable by heterodyne spectroscopy. This implies that the millimeter line observed by Greaves et al. (2020) must be formed relatively high in the mesosphere. An analogy can be drawn with the millimeter lines of SO₂ and SO, formed at about 80 km (Sandor et al., 2010), whose presence requires the existence in the upper mesosphere of a sulfur reservoir, still not identified. On the other hand, it must be reminded that the TEXES data, when using very weak lines, probe only the few kilometers above the cloud top; they are not sensitive to levels higher than about ten kilometers above this level (Encrenaz et al. 2013). The analysis of the constraints provided by the ALMA and TEXES observations on the vertical profile of the observed millimeter line will be the subject of a forthcoming publication. We also note that the narrow width of the PH₃ 1-0 line could possibly be attributed to the removal of the line wings during the process of removing the baseline ripples, which could narrow the line core (Greaves et al 2020, in preparation).

Another explanation for the discrepancy could be the variability of phosphine. Mesospheric sulfur species observed in the

millimeter range (SO, SO₂) are known to vary as a function of time and space (Sandor et al. 2010; Encrenaz et al. 2015b; Piccialli et al. 2017). In any case, the detection of at least one other PH₃ transition, in the infrared or in the millimeter/sub-millimeter range, is definitely needed to confirm the PH₃ detection in Venus.

Acknowledgements. TE, TKG et RG were visiting astronomers at the NASA Infrared Telescope Facility, which is operated by the University of Hawaii under Cooperative Agreement no. NNX-08AE38A with the National Aeronautics and Space Administration, Science Mission Directorate, Planetary Astronomy Program. We wish to thank the IRTF staff for the support of TEXES observations. This work was supported by the Programme National de Planétologie (PNP) of CNRS/INSU, co-funded by CNES. TKG acknowledges support of NASA Grant NNX14AG34G. TE and BB acknowledge support from CNRS. TF acknowledges support from Sorbonne Université. TW acknowledges support from the University of Versailles-Saint-Quentin and the European Commission Framework Program FP7 under Grant Agreement 606798 (Project EuroVenus). We thank E. Lellouch and J. Lequeux for helpful comments regarding this letter.

References

- Belyaev, D. A., Montmessin, F., Bertaux, J.-L. et al. (2012) *Icarus* 217 740
 Bézard, B. and DeBergh, C. (2007) *J. Geophys. Res.* 112, E04S07
 Encrenaz, T., Greathouse, T. K., Richter, M. J. et al. (2008). *Icarus* 179, 43
 Encrenaz, T., Greathouse, T. K., Roe, H. et al. (2012). *Astron. Astrophys.* 543, A153
 Encrenaz, T., Greathouse, T. K., Richter, M. J. et al. (2013). *Astron. Astrophys.* 559, A65
 Encrenaz, T., Greathouse, T. K., Lefèvre, F. et al. (2015a) *Astron. Astrophys.* 578, A127
 Encrenaz, T., Moreno, R., Moullet, A. et al. (2015b). *Plan. Space Sci.* 113, 275
 Encrenaz, T., Greathouse, T. K., Richter, M. J. et al. (2016). *Astron. Astrophys.* 595, A74
 Encrenaz, T., Greathouse, T. K., Marcq, E. et al. (2019). *Astron. Astrophys.* 623, id.A70
 Encrenaz, T., Greathouse, T. K., Marcq, E. et al. (2020). *Astron. Astrophys.* 639, id.A69
 Esposito, L. W., (1984). *Science*. 223, 1072-1074.
 Esposito, L. W., Bertaux, J.-L., Krasnopolsky, V. et al. (1997). Chemistry of lower atmosphere and clouds. in *Venus II: Geology, Geophysics, Atmosphere, and Solar Wind Environment* (eds Bougher, S. W., Hunten, D. M. and Phillips, R. J.) 415
 Fedorova, A., Korablev, O., Vandaele, A.-C. et al. (2008). *J. Geophys. Res.* 113, E00B25
 Greaves, J., Richards, A. M. S., Bains, W. et al. (2020). *Nature Astronomy*, DOI: 10.1038/s41550-020-1174-4
 Jacquinet-Husson, N., Armante, R., Scott, N. A. et al. (2016). *J. Mol. Spectr.* 327, 31
 Krasnopolsky, V. A. (1986) *Photochemistry of the atmospheres of Mars and Venus* (New York: Springer-Verlag)
 Krasnopolsky, V. A. (2007) *Icarus* 191, 25
 Krasnopolsky, V. A. (2010) *Icarus* 209, 314
 Lacy, J. H., Richter, M. J., Greathouse, T. K. et al. (2002). *Pub. Astron. Soc. Pac.* 114, 153
 Marcq, E., Bertaux, J.-L., Montmessin, F. et al. (2013). *Nature Geoscience* 6, 25
 Marcq, E., Jessup, K. L., Baggio, L. et al. (2020) *Icarus* 335, 11386
 Mills, F. P., Esposito, L. W., and Yung, Y. K. (2007), in *Exploring Venus as a Terrestrial Planet*, Geophysical Monograph Series, 176, 73
 Nakazawa, T. and Tanaka, M. (1982) *J. Quant. Spectr. Rad. Transf.* 28, 409
 Piccialli, A., Moreno, R., Encrenaz, T. et al. (2017). *Astron. Astrophys.* 606, A53
 Rohlf, K. and Wilson, T. L. (2004) *Tools for radioastronomy*, 4th edition (Berlin: Springer)
 Sandor, B. J., Clancy, R. T., Moriarty-Schiven, G., Mills, F. P. (2010) *Icarus* 208, 49
 Vandaele, A.-C., Korablev, O., Belyaev, D. et al. (2017a) *Icarus* 295, 16
 Vandaele, A.-C., Korablev, O., Belyaev, D. et al. (2017b) *Icarus* 295, 1
 Wilzewski, J. S., Gordon, I. E., Kochanov, R. V. et al. (2016) *J. Quant. Spectr. Rad. Transf.* 168, 193
 Zhang, K., Liang, M. C., and Mills, F. P. (2012) *Icarus* 217, 714
 Zasova, L. V., Moroz, V. I., Esposito, L., W. and Na, C. Y. (1993) *Icarus* 105, 92